Evidence for methane isotopic bond re-ordering in gas reservoirs sourcing cold seeps from the Sea of Marmara

T Giunta, Jabrane Labidi, I E Kohl, L Ruffine, J P Donval, L Géli, M N Çağatay, H Lu, E D Young

HAL Id: hal-03209518
https://hal.science/hal-03209518

Submitted on 27 Apr 2021

1 **Evidence for methane isotopic bond re-ordering in gas reservoirs sourcing cold**

2 **seeps from the Sea of Marmara**

3 T. Giunta[1,2*], J. Labidi[3**], I.E. Kohl[3***], L. Ruffine[1], J.P. Donval[1], L. Géli[1], M. N.

4 Çağatay[4], H. Lu[5], E.D. Young[3]

5

6 1: IFREMER, Unité des Géosciences Marines, 29280 Plouzané, France

7 2: Université de Bretagne Occidentale, Laboratoire Géosciences Océan, 29280 Plouzané, France

8 3: University of California Los Angeles, Department of Earth, Planetary and Space Sciences, CA 90095 Los Angeles, USA

9 4: Istanbul Teknik University, Faculty of Mines, Department of Geological Engineering, TR-34469 Istanbul, Turkey

10 5: Peking University, Department of Energy & Sciences, College of Engineering, Beijing 100871, China

11

12 *Corresponding author: thomas.giunta@univ-brest.fr

13 ** Now at Institut de Physique du Globe de Paris, Laboratoire de Géochimie des Isotopes Stables, 75005 Paris, France

14 *** Now at Thermo Fisher Scientific (Bremen) GmBH, Hanna-Kunath Str. 11 28199, Bremen, Germany

15

16 **Abstract**

17 **The measurement of methane clumped isotopologues ($\Delta^{13}CH_3D$ and $\Delta^{12}CH_2D_2$) allows exploring**

18 **isotope bond ordering within methane molecules, and may reveal equilibrium temperatures. Whether**

19 **such temperature reflects the formation or re-equilibration temperature of the methane is not well**

20 **understood, but would have critical implications for the use of methane clumped isotopologues as geo-**

21 **thermometers. Here we investigate gas bubbles from vigorous emissions at cold seeps (n = 14) in the Sea of**

22 **Marmara, Turkey. These cold seeps are sourced from deeper sedimentary reservoirs. Conventional**

23 **geochemical tracers such as carbon and hydrogen bulk isotopic ratios ($^{13}C/^{12}C$ and D/H) or *n*-alkane**

24 **molecular ratios, suggest these gases reflect various degrees of mixing between thermogenic and microbial**

25 **sources. Some samples would generally be considered purely microbial in origin ($C_1/C_{2+} > 1500$; $\delta^{13}C <$ -**

26 **60 ‰). We report measurements of $\Delta^{13}CH_3D$ and $\Delta^{12}CH_2D_2$ showing that a fraction of those gases are in**

27 **internal thermodynamic equilibrium, with the abundances of the two mass-18 isotopologues indicating**

28 **concordant temperatures of ~90 °C and ~130 °C . These concordant temperatures are recorded by gases**

29 **of putative microbial and thermogenic origin; the temperatures of equilibration are irrespective of the**

30 **formation mechanism of the gases. We conclude that the two high-temperatures recorded by $\Delta^{13}CH_3D$ and**

$\Delta^{12}CH_2D_2$ are best explained by non-enzymatic re-equilibration at two local subsurface temperatures. First principles suggest that unequal rates of exchange is possible. Disequilibrium signatures where the two isotopologues yield discordant apparent temperatures are exhibited by other samples. In those cases the data define a trend of variable $\Delta^{13}CH_3D$ at nearly constant $\Delta^{12}CH_2D_2$. These signatures are enigmatic, and we investigate and reject multiple possible explanations including mixing, diffusion or Anaerobic Oxidation of Methane. Different rates of re-equilibration between the two rare isotopologues is implied, although lacks experimental foundation at present. In general, all of these data point towards re-equilibration of the mass-18 methane isotopologues as an important process.

1. Introduction

In most natural settings, the generation of hydrocarbon gases results from the degradation in the subsurface of organic-rich sedimentary horizons, either through thermocatalytic cracking (i.e. referred as thermogenic generation), or through microbial reduction of oxidized carbon-bearing species (i.e. microbial methanogenesis). Geochemical investigations of methane and other light hydrocarbons have historically been undertaken using bulk stable isotope ratios of carbon and hydrogen ($\delta^{13}C$ and δD), as well as molecular ratios of light *n*-alkanes (e.g. Bernard et al., 1976; Schoell, 1988). For example, thermogenic gases are expected to contain methane and variable (but significant) amount of C_{2+} gases (i.e. non-methane *n*-alkanes), with $\delta^{13}C$ and δD values evolving as a function of the thermal maturity (Schoell, 1988; Tang et al., 2000) whereas microbial gases are overwhelmingly composed of methane (Martini et al., 1998) with $\delta^{13}C$ and δD being generally lower than methane of thermogenic origin.

Recent advances in high-resolution mass-spectrometry and in laser absorption spectroscopy have allowed the measurement of the relative abundances of doubly-substituted methane isotopologues (i.e. methane molecules containing two heavy isotope substitutions) $^{13}CH_3D$ (Stolper et al., 2014a; Ono et al., 2014; Young et al., 2016) and $^{12}CH_2D_2$ (Young et al., 2016; Eldridge et al., 2019; Gonzalez et al., 2019). These abundances are usually reported as per mil deviations from the "stochastic" isotopologue

56 abundances that would occur with random distributions of isotopes across all species, $\Delta^{13}CH_3D$ and

57 $\Delta^{12}CH_2D_2$. This novel approach allows the investigation of isotope bond ordering in methane

58 molecules. At thermodynamic equilibrium $\Delta^{13}CH_3D$ and $\Delta^{12}CH_2D_2$ provide independent measurements

59 of temperature of formation or equilibration. Where the two temperatures do not agree, kinetic

60 processes or mixing is implied.

61   Rare mass-18 methane isotopologues have been shown to provide apparently reliable formation

62 temperatures in numerous natural settings, from thermogenic (Stolper et al., 2014b; 2015; Wang et al.,

63 2015, Douglas et al., 2016; Young et al., 2017; Giunta et al., 2019), to hydrothermal (Wang et al., 2015,

64 2018) and even possibly to some microbially-dominated settings (Stolper et al., 2015; Wang et al.,

65 2015; Inagaki et al., 2015). Yet, the idea that methane 'clumped' isotopes would reflect the formation

66 temperature requires that methane is synthesized at thermodynamic equilibrium. This later requirement

67 is puzzling because methane generation, whether thermogenic, microbial or abiotic, is always

68 considered to be controlled by kinetic effects rather than by thermodynamic equilibrium (e.g. Berner

69 and Faber, 1996; McCollom, 2013). In the laboratory, the role of kinetic isotope effects on clumped

70 isotopes is clear, especially for microbial generation, and laboratory experiments generally yield

71 disequilibrium signatures (Stolper al., 2015; Wang et al., 2015; Douglas et al., 2016; Young et al., 2017;

72 Shuai et al., 2018; Gruen et al., 2018; Giunta et al., 2019), belying temperature information. Note that

73 these disequilibrium signatures associated with microbial or low-temperature abiotic methane are also

74 observable in nature, especially when measurements of both $\Delta^{13}CH_3D$ and $\Delta^{12}CH_2D_2$ are combined

75 (Young et al., 2017; Giunta et al., 2019). In contrast, thermogenic methane in sedimentary basins seems

76 to show evidence for equilibrium relative abundances of CH_4 isotopologues (Young et al., 2017,

77 Giunta et al., 2019) and it is unclear whether this could reflect a formation temperature or a re-

78 equilibration that occurred after formation.

79   In this study, we investigate methane emitted from vigorous free-gas vents at cold seep sites in

80   the Sea of Marmara (SoM, see Fig. 1) (Geli, et al., 2008; Bourry et al., 2009; Ruffine et al., 2018a).

81   These vents are sourced by underlying sedimentary reservoirs (Ruffine et al., 2018b; Géli et al., 2018).

82   Combining gas composition with carbon and hydrogen stable isotope analyses, two main origins of gas

83   were identified (Ruffine et al., 2018b). Gases sampled on the structural highs, the Western High and

84   Central High, are thought to be thermogenic in origin, whereas gases sampled in the southern flank of

85   the Tekirdağ Basin and in the Çinarcik Basin are thought to be essentially microbial in origin. Other

86   gases from the area were interpreted to reflect various proportions of mixing between these two types

87   of sources. Hydrate formation or destabilization is unlikely to have affected these gases. All gases were

88   collected at locations where thermodynamic conditions for hydrate stabilization are not met with the

89   exception of samples collected in the Western High (Ruffine et al., 2012; 2018b). In contrast, the

90   chemical and isotopic compositions have been all accounted for by mixing. Mixing as illustrated in Fig.

91   2 using the methane $\delta^{13}C$ versus C_1/C_{2+} ratios (Ruffine et al., 2018b). Thermogenic gases are typically

92   thought to contain significant amounts of C_{2+} gases and therefore to show low C_1/C_{2+} ratios together

93   with relatively enriched methane $\delta^{13}C$ values (e.g. Bernard et al., 1976). In contrast, microbial gases are

94   expected to be dominated by methane with trace amounts of C_{2+} gases and are therefore expected to

95   have high C_1/C_{2+} ratios together with relatively low $\delta^{13}C$ values. Thus, mixing between thermogenic

96   and a microbial end members is predicted to produce a characteristic mixing hyperbola (Fig. 2). Some

97   samples from the SoM however – especially gases from the Central High and from the western flank of

98   the Tekirdağ Basin – appear to deviate from this mixing line. These gases were noted to show

99   anomalously heavy propane $\delta^{13}C$ (Ruffine et al., 2018b), comprising evidence for biodegradation of

100   propane (James and Burns, 1984) which could explain the departure from the two endmembers mixing

101   line (Fig. 2). In this study, we explore further these hypotheses by combining the measurement of

4

102   $^{13}CH_3D$ and $^{12}CH_2D_2$ to provide additional constraints on the thermal history of methane in the

103   sedimentary reservoirs feeding the Marmara cold vents.

104

105   **2. Geological setting and fluid activity**

106   The Sea of Marmara (SoM) is an interior sea located in the Turkish territory and links the Black

107   sea to the northeast and the Mediterranean sea to the west via the Bosphorus and the Darnaelle straits,

108   respectively. The SoM is composed of three basins, the Tekirdağ Basin, the Central Basin and the

109   Çınarcık Basin, which latter reaches a maximum depth of 1273 m. Each of the basins are separated by

110   push-up structures, the Western High and the Central High (see Fig. 1). The SoM seafloor is cut

111   lengthwise by a dense network of faults belonging to the North Anatolian Fault (NAF) system which

112   accommodates the slip motion between the Eurasian plate and the Anatolian block (e.g. Armijo et al.,

113   1999). In the northern part of this network, the Main Marmara Fault is seismically the most active

114   sequence of fault segments in the region, having caused devastating earthquakes in the past (e.g.

115   Ambraseys and Jackson, 2000).

116   At the seafloor, cold seeps with fluid and gas emissions are widespread across the SoM, but

117   appear to be more frequent near active faults (e.g. Geli et al., 2008), perhaps suggesting a relationship

118   between pressurized gas reservoirs and seismic activity (Gasperini et al., 2011; Geli et al., 2018). The

119   sampling of free-gas (i.e. bubbles) emanating at the SoM seafloot was first achieved during the Marsite

120   cruise in 2007, after detection of gas seep locations using a SIMRAD-EK60 echo sounder and acoustic

121   anomalies associated to gas bubbles in the water column (Geli et al., 2008). At the time, only three

122   active gas sites were sampled in the Çinarcik Basin, in the Western High and in the Central High

123   (Bourry et al., 2009). In 2014, a more extensive study on gases discharged at the SoM seafloor along

124   the NAF was undertaken during the Marsite Cruise (Ruffine et al., 2018a,b). Through combination of

125   acoustic survey and ROV dives, new active sites were discovered and sampled in the Çinarcik Basin, in

126 the Western High and in the Central High, as well as in the Tekirdağ Basin (Ruffine et al., 2018b).

127 Gases that are venting at the seafloor consist mainly of methane-rich mixtures (up to > 99 %-mol),

128 some of which containing significant amount of other hydrocarbon. The contribution of light *n*-alkanes

129 is thought to reflect hydrocarbon formation within sediments in the SoM via organic matter

130 degradation, both thermocatalytic cracking of organic matter and microbial reduction of oxidized

131 carbon-bearing species have been suggested (Gürgey et al., 2005; Ruffine et al., 2018b).

132

133 **3. Methods**

134 Gas samples were collected in the course of the Marsite Cruise in November 2014. Method for

135 gas sampling and preservation are outlined in details in Ruffine et al., (2015, 2018b). Seafloor gas vents

136 were identified by coupling water column acoustic guiding and visual inspection with the ROV Victor

137 6000. The most vigorous gas vents were then sampled with the PEGAZ sampler, a sampling device

138 manipulated by the ROV which is designed to sample gas bubbles and preserve them at *in situ*

139 pressure. Gas aliquots were then sub-sampled at pressure ranging between 2 and 4 bars in 12 mL Labco

140 vials. These Labco vials were then used for measuring the gas composition (light alkanes, N_2 and CO_2

141 contents) as well as bulk isotope geochemistry ($\delta^{13}C$, δD) on light alkane (including methane). All these

142 isotope analyses were performed at ISOLAB in the Netherlands. Results were reported and discussed

143 by Ruffine et al., (2018b).

144 Methane gas samples were purified and analyzed at UCLA to obtain methane isotopologue

145 abundances. The ratios $^{13}CH_3D/^{12}CH_4$, $^{12}CH_2D_2/^{12}CH_4$, $^{13}CH_4/^{12}CH_4$, and $^{12}CH_3D/^{12}CH_4$ are measured

146 with the prototype Nu Instruments Panorama, a high-resolution gas-source double-focusing mass

147 spectrometer at UCLA. Mass-18 isotopologue compositions are reported versus a stochastic

148 distribution (Wang et al., 2004), representing a theoretically infinite temperature, and expressed in per

149 mil using the capital delta notation:

6

150

151     $\Delta^{13}CH_3D = [(^{13}CH_3D/^{12}CH_4)_{sample}/(^{13}CH_3D/^{12}CH_4)_{stochastic} - 1] \times 1000$ (1)

152

153   and

154

155     $\Delta^{12}CH_2D_2 = [(^{12}CH_2D_2/^{12}CH_4)_{sample}/(^{12}CH_2D_2/^{12}CH_4)_{stochastic} - 1] \times 1000$ (2).

156

157 Methods for sample purification and isotope ratio measurements are outlined in detail by Young et al.,

158 (2016, 2017) and briefly summarized here. Prior to measurements of isotopologues, methane is purified

159 on a vacuum line interfaced with a gas chromatograph (GC). Two GC columns are coupled in series

160 using He as the carrier gas. The first column consists of a 3-m long, 1/8-inch OD stainless steel tubing,

161 packed with 5A molecular sieve and is used to separate H_2, Ar, O_2 and N_2 from CH_4 and other alkanes.

162 The second column is used to separate CH_4 from other hydrocarbons and consists of a 2-m long 1/8-

163 inch OD stainless steel tubing packed with HayeSep D porous polymer. Peaks are identified on a

164 passive TCD. In order to measure $^{12}CH_4^+$, $^{13}CH_4^+$, $^{12}CH_3D^+$, $^{13}CH_3D^+$ and $^{12}CH_2D_2^+$ ion currents, the mass

165 spectrometer is set to a mass resolving power equal to or greater than 40000. This allows resolving of

166 the two mass-18 isotopologues ($^{13}CH_3D$ and $^{12}CH_2D_2$), both measured on the axial collector with an

167 electron multiplier. Meanwhile, mass-16 and mass-17 isotopologues are measured on Faraday

168 collectors with amplifier resistors of 10^{11} Ω. Sample and reference bellows are adjusted so that ion

169 current intensities are balanced. The current intensities are rebalanced after each measurement cycle. At

170 first, the magnet is set to measure simultaneously $^{12}CH_3D^+/^{12}CH_4^+$ and $^{12}CH_2D_2^+/^{12}CH_4^+$ ratios, with

171 $^{12}CH_2D_2^+$ (18.04385 amu) being measured on the axial collector. In a second setting, the magnet is set to

172 measure $^{13}CH_3D^+$ (18.04090 amu) on the axial collector, and $^{13}CH_4^+/^{12}CH_4^+$ and $^{13}CH_3D/^{12}CH_4^+$ ratios are

173 measured simultaneously. Overall, the external 1σ error (n= 5) including both the accuracy and the

174 reproducibility is estimated to be ± 0.1 ‰ for $\Delta^{13}CH_3D$, ± 0.8 ‰ for $\Delta^{12}CH_2D_2$, ± 0.1 ‰ for $\delta^{13}C$, and

175 of approximately ± 0.3 ‰ for δD. Note that the measurements of methane $\delta^{13}C$ and δD values

176 performed conjointly with the rare methane isotopologues are within uncertainties of measurements

177 previously performed at ISOLAB.

178

179 **4. Results**

180 The measurements of $\Delta^{13}CH_3D$ and $\Delta^{12}CH_2D_2$ allow the description of methane isotopic bond-

181 ordering in a given sample. At thermodynamic equilibrium both $\Delta^{13}CH_3D$ and $\Delta^{12}CH_2D_2$ should be

182 concordant in recording the same temperature of equilibrium. The data are shown in Figure 3, together

183 with the theoretical thermodynamic equilibrium curve (Young et al., 2016). Samples DV04-PE02,

184 DV04-PE08, DV01-PE02, DV03-PE03 and DV05-PE02 appear close to equilibrium, though they show

185 two populations of $\Delta^{13}CH_3D$ and $\Delta^{12}CH_2D_2$ values (Fig. 3b). The first group composed of samples

186 DV03-PE03 and DV05-PE02 define average $\Delta^{13}CH_3D$ and $\Delta^{12}CH_2D_2$ values of 3.45 ± 0.1 ‰ and

187 8.88 ± 0.4 ‰ yielding apparent concordant temperatures of $127^{+5}_{-5}°C$ and $135^{+7}_{-7}°C$, respectively.

188 These consistent temperatures are indistinguishable, and suggest that isotope ordering was in response

189 to thermodynamic equilibrium in these samples. The second group composed of samples DV01-PE02,

190 DV04-PE02 and DV04-PE08, define average $\Delta^{13}CH_3D$ and $\Delta^{12}CH_2D_2$ of 4.40 ± 0.16 ‰ and

191 11.96 ± 0.32 ‰, yielding nearly concordant apparent temperatures of $77^{+7}_{-8}°C$ and $92^{+4}_{-4}°C$, respectively.

192 The remaining samples appear shifted to the right of the equilibrium curve to varying degrees, i.e. they

193 show higher $\Delta^{13}CH_3D$ values at a given $\Delta^{12}CH_2D_2$ relative to equilibrium (Fig. 3b). For these, it is not

194 clear whether any temperature information can be *a priori* obtained from either $\Delta^{13}CH_3D$ or $\Delta^{12}CH_2D_2$.

195 Probability density plots indicate that the distribution of $\Delta^{12}CH_2D_2$ values is bi-modal (Fig. 3b), with

196 peaks at 8.01 ± 1.08 ‰ and 11.88 ± 0.44 ‰, corresponding to apparent temperatures of 152±22 °C and

197 93±5 °C, respectively. These two temperatures are remarkably similar to maximum temperatures

8

198 reached by two main source rocks in the area, the Eocene Hamitabad Formation and the Oligocene

199 Mezardere Formation (Huvaz et al., 2005; Gürgey, 2009).

200   Samples from the western flank of the Tekirdağ Basin (DV03) may be taken as a telling

201 illustration of the overall complexity of our dataset. These gases show the widest variability in methane

202 doubly-substituted isotopologue signatures, with $\Delta^{13}CH_3D$ ranging from 3.4 to 6.3 ‰, and $\Delta^{12}CH_2D_2$

203 ranging from 5.7 to 11.2 ‰. These samples also show the largest variability in C_1/C_{2+} values ranging

204 from 10 to 1560 (Fig. 2), and bulk $\delta^{13}C$ ranging from -41.2 to -58 ‰ (Fig. 2, Fig.3a). However,

205 perhaps most curious is that two samples, DV03-PE01 and DV03-PE06 are nearly identical both in

206 their gas composition and in their bulk isotopic signatures (Fig. 2, Fig. 3a), and yet show significantly

207 different $\Delta^{13}CH_3D$ values at a given $\Delta^{12}CH_2D_2$, being members of the two distinct groups defined by the

208 two peaks in $\Delta^{12}CH_2D_2$ values (Fig. 3b). This is also true for samples from the Çinarcik Basin (DV05)

209 and, though less significant, for samples from the southeastern flank of the Tekirdağ Basin (DV04. All

210 of these samples have been previously interpreted as dominantly microbial in origin (Ruffine et al.,

211 2018). In other words, we observe a decoupling between conventional tracers and clumped methane

212 signatures.

213   Decoupling also appears for some samples which are distinct in gas composition and in bulk

214 isotope signatures but are similar in the isotopologue space (Fig. 3b). The most striking case are the

215 DV03-PE03 (Tekirdağ Basin) and the DV05-PE02 (Çinarcik Basin) samples. They both plot on (or

216 near) the equilibrium curve at an equivalent temperature of ~130°C. However, they have distinct bulk

217 isotope compositions. Sample DV03-PE03 shows relatively high $\delta^{13}C$ (of -41.2 ‰) together with low

218 C_1/C_{2+} (of 10) which could reflect a thermogenic end-member (Ruffine et al., (2018b) similar to oil-

219 associated gases found in the Thrace Basin (Huvaz et al., 2005; Gürgey, 2009). An apparent

220 equilibrium temperature of ~130°C derived from both $\Delta^{13}CH_3D$ and $\Delta^{12}CH_2D_2$ would indicate a

221 temperature generally consistent with the typical range expected for thermogenic gas generation (Tissot

222   and Welte, 1978). On the other hand, based on the lack of C_{2+} ($C_1/C_{2+} = 1456$) and low $\delta^{13}C$ and δD

223   values -63 ‰ and -251 ‰ respectively, sample DV05-PE02 appears microbial in origin (i.e. derived

224   from microbial methanogenesis). For this sample, apparent temperatures of ⟨...⟩ and 139^{+14}_{-13} °C,

225   derived from $\Delta^{13}CH_3D$ and $\Delta^{12}CH_2D_2$ respectively, are within uncertainty of the upper temperature limit

226   for life of ~ 121 °C (Kashefi and Lovley, 2003; Takai et al., 2008).

227   Overall, variations observed in the $\Delta^{13}CH_3D$ and $\Delta^{12}CH_2D_2$ space do not correlate with bulk

228   isotope ratios or in C_1/C_{2+}. This suggests that the isotope bond ordering is responding to forcings that

229   are not obviously related to gas composition or bulk isotope ratios.

230

231   **5. Discussion**

232   5.1. Isotope-bond reordering

233   First studies on methane isotopologues have provided consistent observations when

234   investigating methane of thermogenic or microbial origin. Apparent agreement between $\Delta^{13}CH_3D$-

235   based temperatures and measured environmental temperatures, or expected formation temperatures

236   were observed for most thermogenic gases (Stolper et al., 2014b, 2015, 2017; Wang et al., 2015;

237   Douglas et al., 2016). In addition, concordant temperature from both $\Delta^{12}CH_2D_2$ and $\Delta^{13}CH_3D$ in the

238   same samples supports the idea that thermogenic methane in natural settings is generally at 'bond

239   ordering' equilibrium (Young et al., 2017; Giunta et al., 2019). Yet, the mechanism by which

240   isotopologues reach equilibrium in nature is still unclear, as thermogenic generation is generally

241   thought to be controlled by kinetics (e.g. Clayton, 1991; Tang et al., 2000; Stolper et al., 2017; Xia and

242   Gao, 2019). Recently, experimental and modeling works have also shown that disequilibrium

243   signatures could be expected during gas generation and/or accumulation in reservoirs (Shuai et al.,

244   2018; Xia and Gao, 2019), yet it does not seem to be common in most natural settings.

245   On the other hand, microbial methane is associated with large isotopologue disequilibrium

246   under laboratory conditions, often yielding negative $\Delta^{13}CH_3D$ (Wang et al., 2015; Stolper et al., 2015;

247   Young et al., 2017; Douglas et al., 2017 Gruen et al., 2018; Giunta et al, 2019) and markedly negative

248    $\Delta^{12}CH_2D_2$ values (Young et al., 2017; Giunta et al, 2019; Gonzalez et al., 2019) (Fig. 4). The causes of

249   the disequilibrium are beyond the scope of this study but may include: the rate of methanogenesis (e.g.

250   Wang et al., 2015, Stolper et al., 2015), the metabolic pathways (Giunta et al., 2019; Young 2019),

251   statistical combinatorial effects (Young et al., 2017; Cao et al., 2019; Taenzer et al., 2020), and/or

252   quantum tunneling effects (Young et al., 2017; 2019). In natural settings, disequilibrium signatures

253   similar to those observed in laboratory are commonly observed (e.g. Wang et al., 2015; Douglas et al.,

254   2016; Giunta et al., 2019; Young, 2019), however, there are certain environments, such as in marine

255   sediments, where isotopologue signatures appear closer to equilibrium with environmental

256   temperatures (e.g. Wang et al., 2015; Stolper et al., 2015; Douglas et al., 2016; Inagaki et al., 2015;

257   Giunta et al., 2019; Ash et al., 2019). This led some authors to propose that isotopologue signatures

258   during microbial methanogenesis would be largely controlled by the degree of metabolic reversibility

259   (Wang et al., 2015; Stolper et al., 2015), and may sometimes, especially in the deep biosphere, result in

260   methane in isotopologue equilibrium. Young et al. (2017) argued that microbial communities may drive

261   methane towards equilibrium in nature, and Young (2019) presented preliminary evidence for the

262   potential role of methanotrophic organisms performing Anaerobic Oxidation of Methane (AOM) in re-

263   ordering atomic bonds within methane molecules towards the equilibrium (also supported by Giunta et

264   al., 2019). Ash et al. (2019) presented evidence that AOM causes methane to achieve equilibrium

265    $\Delta^{13}CH_3D$ and $\Delta^{12}CH_2D_2$ values in the sediments from the Bornholm Basin, Baltic Sea. Both proposed

266   mechanisms for equilibration lack unequivocal experimental validation at present.

267   In SoM gases, samples DV03-PE03 and DV01-PE02 were identified as dominantly

268   thermogenic in origin (Ruffine et al., 2018b) and define two distinct but concordant temperatures of

269 ~130 °C and ~90 °C, respectively (Fig. 3b). Both temperatures are consistent with the 'gas window' for

270 thermogenic generation (Tissot and Welte, 1978) and with maximum temperatures reached by two

271 main source rocks in the area, the Eocene Hamitabad Formation and the Oligocene Mezardere

272 Formation (Huvaz et al., 2005; Gürgey, 2009). We therefore interpret these data as recording

273 characteristic regional temperatures for methane equilibration.

274   In contrast, samples DV05-PE02, DV04-PE02 and DV04-PE08 are considered to be dominantly

275 microbial in origin on the basis of $\delta^{13}C$ < -60 ‰ and C_1/C_{2+} > 1000, but nonetheless plot on (or near)

276 the equilibrium curve at temperatures of ~90 and ~130 °C, the same two temperatures recorded by the

277 thermogenic samples (Fig. 3b). It is unlikely that these relatively high temperatures for nominally

278 microbial gases are the result of hyper-thermophilic activity in sediments of the SoM. A temperature of

279 ~130 °C slightly exceeds the upper temperature limit for life of ~ 121 °C, a maximum that has so far

280 only been observed for optimal laboratory conditions and for archeal strains that are typical of energy-

281 rich hydrothermal vent environments (Kashefi and Lovley, 2003; Takai et al., 2008). The temperature

282 limit for microbial degradation of organic matter in subsurface sedimentary settings that are nutrient-

283 starved systems [REF] is considered to be 80-90°C (Head et al., 2003), and possibly even lower at

284 ~60 °C in deeply buried sediments (Inagaki et al., 2015). For these reasons, we conclude that an

285 equilibrium temperature of ~ 130 °C for natural methane with microbial traits must necessary reflect a

286 'non-enzymatic' (i.e. abiotic) re-equilibration to a temperature reached during sediment burial, rather

287 than the actual temperature of formation of microbial methane in the subsurface. This explanation may

288 also hold true for putative microbial methane equilibrated at temperatures of ~ 90 °C (DV04-PE04 and

289 DV04-PE08). The implication is that the production and accumulation of microbial methane occurred

290 prior to burial, after which it re-equilibrated upon the heating that attended burial. Accordingly, we this

291 can not exclude that thermogenic gases now appearing on the equilibrium $\Delta^{12}CH_2D_2$ vs. $\Delta^{13}CH_3D$ curve

have inherited their equilibrium signature from a similar re-equilibration mechanism, rather than from their actual formation.

Rates for re-equilibration of $^{13}CH_3D/^{12}CH_4$ and $^{12}CH_2D_2/^{12}CH_4$ isotopologue ratios, especially at relatively low temperatures, are unknown. Wang et al., (2018) have speculated that rates for re-equilibration of $^{13}CH_3D$ may follow the rates for 'external', or inter-species re-equilibration of D/H ratios between methane and water in hydrothermal systems. They extrapolated from a small body of experimental data at 200, 323 and 400 °C that the timescale for CH_4 isotopic bond re-ordering in the absence of a metal catalyst would be on the order of 10^9 years for temperature of 150 °C, and $> 10^{10}$ years below 100 °C. This would suggest that the relative abundances of methane isotopologues are not subject to resetting in most sedimentary settings. This conclusion appears to be contradicted by our observations. In fact, our dataset argues in favor of faster isotopologue re-ordering rates than those for inter-species isotope exchange with environmental (reservoir) waters. Our data requires that methane re-equilibration at rather cool (< 150 °C) subsurface conditions can occur, promoted or catalyzed by a mechanism that remains to be identified. Recently, a similar process was suggested to account for $^{12}CH_2D_2$ re-ordering down to 65 °C with no resolvable $^{13}CH_3D$ re-equilibration in well characterized marine hydrothermal vent fluids (Labidi et al., 2020).

From this data-set, it is clear that we cannot determine with certainty whether methane achieved bond equilibrium via exchange with other molecules. Source reservoirs are not readily accessible to sampling, precluding assessments of inter-species (e.g., CH_4 and H_2O) isotopic exchange. The fact that samples DV05-PE02 and DV05-PE03 have identical δD values, but distinct $\Delta^{13}CH_3D$ values, one at equilibrium based on concordance with $\Delta^{12}CH_2D_2$, and the other not, may indicate that re-equilibration among methane molecules can occur without significant isotope exchange with other molecular species that would cause shifts in the methane bulk δD values. The alternative is that these two samples have reached D/H equilibrium with the same source of hydrogen but did not reach mass-18 isotopologue

13

316 equilibrium. In either case, it appears as though rates for bond re-equilibration and for inter-species re-

317 equilibration are decoupled.

318 The probability distributions in Fig. 3b suggest that $\Delta^{12}CH_2D_2$ has experienced a greater degree

319 of re-equilibration than $\Delta^{13}CH_3D$. We investigate the prospects for this in greater detail in Section

320 5.2.4. The catalysis of hydrogen isotope exchange among alkanes has been studied for almost a century

321 (see recent review by Sattler, 2018), but remains poorly understood for temperatures and timescales

322 that might be relevant for geological applications. Transition metals are well known to catalyze

323 hydrogen exchange with methane (Horibe and Craig, 1995) and have been shown to promote

324 isotopologue equilibrium at temperatures above 150 °C (Stolper et al., 2014; Ono et al., 2014; Young et

325 al., 2016). Recent studies have also demonstrated the potential of aluminum oxide (in the form of γ-

326 alumina) in promoting re-equilibration of methane to temperatures as low as 1 °C (Wang et al., 2019;

327 Eldridge et al., 2019). In both cases, it is not clear how this type of catalysis can be relevant to

328 sedimentary environments. Alternatively, exchange mediated by clay mineral surfaces might be a

329 process to consider, as clays are known to promote hydrogen exchange on larger organic molecules

330 (Alexander et al., 1982, Sessions et al., 2004).

331

332 5.2. Departures from Equilibrium

333 *5.2.1. Mixing*

334 Methane samples that do not record concordant temperatures of ~90 and ~130 °C exhibit

335 variable but significant degrees of disequilibrium, all plotting to the right of the equilibrium curve in

336 Fig. 3b and exhibiting relatively large variations in $\Delta^{13}CH_3D$ and relatively small variations in

337 $\Delta^{12}CH_2D_2$. Based on bulk isotope ratios and molecular ratios, these gases may have $\Delta^{12}CH_2D_2$ and

338 $\Delta^{13}CH_3D$ values resulting from mixing between thermogenic and microbial gases (Fig. 2; Ruffine et al.,

339 2018b). However, mixing, if it occurred, may now be disguised by varying degrees of re-equilibration

340 based on the evidence summarized in Fig. 3b. Nonetheless, vestiges of disequilibrium in isotopologue

341 space due to mixing may persist. In general, the samples showing the largest offset from the

342 equilibrium curve (DV03-PE01, DV03-PE09 and DV05-PE03) are considered to be dominantly

343 microbial in origin based on bulk isotope ratios and the molecular concentrations comprising the gas.

344 This suggests that one end-member for mixing was microbial, perhaps having $\Delta^{12}CH_2D_2$ and $\Delta^{13}CH_3D$

345 values characteristic of microbial methanogenesis in the laboratory and in some natural settings. The

346 magnitude of the disequilibrium observed in our data is much less than that obtained from microbial

347 methanogenesis in laboratory cultures (Young et al., 2017) and from samples of microbial

348 methanogenesis origin in natural settings investigated to date where both $\Delta^{13}CH_3D$ with $\Delta^{12}CH_2D_2$ have

349 been measured (Giunta et al., 2019; Young 2019) (Fig. 4). Invoking a microbial end-member with a

350 signature similar to those measured in the laboratory would imply that the most disequilibrated samples

351 in this study are composed of no more than 40 to 60 % microbial methane (Fig. 4). While mixing of

352 this end-member with a thermogenic component explains the isotopologue data (Fig. 4), this relatively

353 low fraction of microbial methane would be inconsistent with their $C_1/C_{2+} > 1000$ usually considered

354 indicative of a nearly pure microbial origin (e.g. Bernard et al., 1976). This observation may in turn

355 suggest that microbial methane in deep biosphere do necessarily resemble laboratory cultures (e.g.

356 Wang et al., 2015; Stolper et al., 2015; Douglas et al., 2016; Giunta et al., 2019).

357   Gases from the Western High (DV02-PE01 and PE02) identified as mainly thermogenic also

358 have disequilibrium $\Delta^{13}CH_3D$ and $\Delta^{12}CH_2D_2$ values (Fig. 3b.) while showing little evidence of a

359 microbial contribution (low C_1/C_{2+} of ~15). Therefore, thermogenic gases may also have contributed to

360 disequilibrium $\Delta^{13}CH_3D$ and $\Delta^{12}CH_2D_2$ values in mixtures. Deciphering the impact of mixing is

361 exacerbated by a lack of correlation between C_1/C_{2+} and disequilibrium isotopologue signatures (Fig 5).

362 In any event, the $\Delta^{13}CH_3D$ and $\Delta^{12}CH_2D_2$ data from the SoM fail to follow a simple two-component

363 mixing in which thermogenic gases with low C_1/C_{2+} ratios are mixed with microbial gases with

15

364 elevated C_1/C_{2+} ratios. Mixing does not seem to be the primary cause of variable mass-18 isotopologues

365 in these samples.

366

367 *5.2.2 Mass-dependent fractionation during migration*

368 An alternative explanation for the disequilibrium trend of highly variable $\Delta^{13}CH_3D$ values and

369 relatively minor variations in $\Delta^{12}CH_2D_2$ is mass fractionation of the SoM gases during their migration

370 in the subsurface (i.e. for example from source rock to reservoir or from reservoir to reservoir) and/or

371 to the seafloor. Though migration of free gas (bubbles) to the seafloor is an advective process and is

372 therefore not a mechanism for fractionating isotopologues, diffusive transport prior to gas saturation

373 can segregate methane molecules according to their masses. Diffusion favors the light isotopologues

374 for the diffused gas (as opposed to the residual gas) resulting in decreases in $\delta^{13}C$ and δD values but

375 increases in $\Delta^{13}CH_3D$ and $\Delta^{12}CH_2D_2$ values. In $\Delta^{12}CH_2D_2$ vs. $\Delta^{13}CH_3D$ space both axes refer to the same

376 integer mass ratio of 18/16, and any fractionation by molecular mass, including by diffusion, should

377 produce a 1:1 slope in this space (Young et al., 2017). A 1:1 relationship is also expected for gases

378 affected by diffusion in δD vs. $\delta^{13}C$ space since both axes refer to integer mass ratios of 17/16. In the

379 SoM gas samples, the slope-1 relationship expected between $\delta^{13}C$ and δD values by mass segregation

380 according to molecular weight is only crudely evident when taken in aggregate (Fig. 6a). However, the

381 data are more consistent with a diffusive fractionation process if one considers that $\Delta^{13}CH_3D$ and

382 $\Delta^{12}CH_2D_2$ are distributed along two distinct diffusion trends starting from two equilibrium temperatures

383 of about ~100 and 200 °C (Fig. 6b). These temperatures are at the high-temperature ends of the two

384 groups of samples shown in Fig. 3b.

385 If diffusion is at play, samples showing the largest offset from the equilibrium curve in mass-18

386 isotopologue space should be relatively low in bulk $\delta^{13}C$ and δD. In detail however, when assigning

387 self-consistent diffusion coefficients to all methane isotopologues, it appears that an enrichment of

16

388 > 3 ‰ in $\Delta^{13}CH_3D$ as observed in our data should be associated with a shift in bulk $\delta^{13}C$ by ~ -50 ‰

389 (Fig. 6c). This is not observed; our entire suite of data do not range over more than ~ 25 ‰ in $\delta^{13}C$, so

390 that the overall observed range of variations in $\Delta^{13}CH_3D$ appears intrinsically inconsistent with

391 diffusion (or any mass-dependent process) being a dominant mechanism at play in the subsurface of the

392 SoM. We conclude that diffusion is not a principal mechanism affecting the mass-18 isotopologue

393 abundances in our methane samples.

394

395 *5.2.3 Microbial methane oxidation*

396 Apparent temperatures inferred from $\Delta^{13}CH_3D$ range from 131^{+6}_{-7}°C (DV03-PE03) to 9^{+3}_{-3}°C (DV03-

397 PE09), perhaps representing a range from a deep reservoir temperature to a near seafloor temperature

398 (~ 14°C) if taken at face value. Thus, one may speculate that venting gases had their $\Delta^{13}CH_3D$ values

399 re-equilibrated during their ascent towards a near-seafloor temperature, without significantly re-

400 equilibrating $\Delta^{12}CH_2D_2$ values. Several recent studies have stressed the potential importance of

401 microbial Anaerobic Methane Oxidation (AOM) in re-ordering isotopic bond associations in methane

402 gas, and thus causing methane to progressively evolve towards equilibrium at ambient temperatures for

403 both mass-18 isotopologues (e.g. Young et al., 2017; Giunta et al., 2019; Ash et al., 2019). The uptake

404 of methane by methanotrophic organisms, in particular by archeal strains performing AOM, is a

405 widespread process generally occurring in the first few meters of marine sediments, thus at a

406 temperature that should not be drastically different from those at the seafloor. AOM has been

407 recognized as a major methane sink in sediments from the SoM (e.g. Crémière et al., 2012), including

408 in those surrounding the gas seeps studied here (Teichert et al., 2018). However, our samples were all

409 collected as free-gas (i.e. bubbles), which is generally considered non-accessible to AOM (Luff and

410 Wallmann 2003; Treude et al., 2003). For AOM to have impacted the gas studied here, it would be

411 required to have occurred prior to gas saturation. AOM is expected to yield a progressive enrichment of

412   both δ^{13}C and δD in the residual methane (e.g. Whiticar, 1999; Holler et al., 2011), however there is no

413   specific relationship between off-equilibrium signature and bulk signatures in our data-set (Fig. 6c may

414   illustrate that too). In marine sediments however, AOM is expected to occur with significant

415   reversibility effects (e.g. Yoshinaga et al., 2014), perhaps implying that a classic kinetic framework is

416   not relevant for this type of settings. The study of methane in shallow sediments from the Bornholm

417   Basin, Baltic Sea, yielded showed evidence for re-equilibration in Δ^{13}CH$_3$D and Δ^{12}CH$_2$D$_2$ to

418   environmental temperature with little effects on the bulk δ^{13}C and δD signatures (Ash et al., (2019).

419   This study suggests that shifts in Δ^{13}CH$_3$D and not Δ^{12}CH$_2$D$_2$, as observed in our data, being the result

420   of AOM is unlikely.

421   A caveat to this conclusion arises because of preliminary experimental results suggesting that

422   AOM under a set of restrictive conditions may yield signatures similar to our disequilibrated samples

423   (Young, 2019). These preliminary results suggest that under low sulfate content (< 1 mM), AOM

424   mediation would re-equilibrate Δ^{13}CH$_3$D to environmental temperatures while maintaining the

425   Δ^{12}CH$_2$D$_2$ virtually unchanged. It is unclear how these results may be extrapolated to marine settings,

426   but the similarity with our data-set suggests that effects on methane isotopologues due to AOM cannot

427   be ruled out entirely. We note that the presence of a largely Δ^{13}CH$_3$D AOM effect driving equilibration

428   towards colder temperatures would not be inconsistent with non-enzymatic re-equilibration as

429   described above. The AOM would simply modify the isotopologue abundances equilibrated at ~90 and

430   ~130 °C, prior to AOM.

431

432   *5.2.4. Different re-equilibration rates for Δ^{13}CH$_3$D and Δ^{12}CH$_2$D$_2$?*

433   In the above sections we have discussed two mechanisms that could cause re-equilibration of

434   methane isotopologue abundances. We suggested that non-enzymatic (i.e. abiotic) intra-methane

435   exchange could cause re-equilibration of microbial (and perhaps thermogenic) gases formed at low

18

436 temperatures to higher temperatures characteristic of known temperatures reached during sediment

437 burial in the area (section 5.1). The bi-modal distribution of $\Delta^{12}CH_2D_2$ values suggests re-equilibration

438 to two distinct temperatures of ~152 °C and ~90 °C that appear consistent with the thermal history of

439 sediments beneath the SoM. Enzymatic (i.e. biotic) facilitated exchange of isotopes among methane gas

440 molecules could have caused $\Delta^{13}CH_3D$ to partially re-equilibrate to near seafloor temperatures, perhaps

441 during gas ascent to the seafloor (section 5.2.3). As discussed before, the bi-modal distribution of

442 $\Delta^{12}CH_2D_2$ data seem to point towards two distinct temperatures of ~152 °C and ~90 °C that appear

443 consistent with the thermal history of sediments beneath the SoM. The variable $\Delta^{13}CH_3D$ data span a

444 range of apparent temperatures from ~130 °C to ~10 °C. Based on these observations, one may

445 speculate that our data illustrate that re-equilibration rates for the relative abundances of $^{13}CH_3D$ and

446 $^{12}CH_2D_2$ may be different.

447 More specifically, the bi-modal $\Delta^{12}CH_2D_2$ values at two geologically plausible temperatures

448 suggest isotopic bond re-ordering to equilibrium or near-equilibrium values, while $\Delta^{13}CH_3D$ values are

449 are more variable, perhaps as a result of only partial re-equilibration. This would imply that $\Delta^{12}CH_2D_2$

450 re-equilibrates faster than $\Delta^{13}CH_3D$, and that $\Delta^{13}CH_3D$ carries a memory of pre-reset conditions. Note

451 this scenario does not allow the microbial methane, prior to re-equilibration, to be as low in $\Delta^{13}CH_3D$ as

452 observed in culture studies (< 4 ‰ ; e.g. Young et al., 2017) and would rather suggest a microbial

453 methane (prior re-equilibration) with $\Delta^{13}CH_3D$ ~ 6 ‰ (equivalent to T ~ 15°C), consistent with the idea

454 of a deep biosphere methane being nearly equilibrated with environmental temperatures in $\Delta^{13}CH_3D$.

455 In order to explain our data as being purely the result of different rates of equilibration for

456 $^{12}CH_2D_2$ and $^{13}CH_3D$, we use a simple kinetic model for exchange. In this model, we consider the intra-

457 methane exchange reaction:

458

459
$$^{12}CH_3D + {}^{12}CH_3D \underset{k_1}{\overset{\alpha_1 k_1}{\rightleftarrows}} {}^{12}CH_2D_2 + {}^{12}CH_4 \qquad (3)$$

19

460
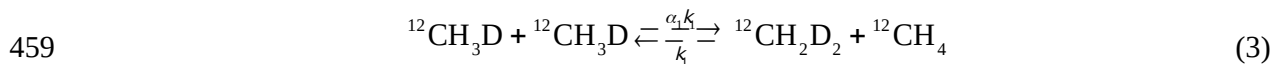
461 where α_1 is the equilibrium fractionation factor and k_1 is the rate constant. A simple rate equation for

462 this reaction is

463

$$\frac{d\left[^{12}CH_2D_2\right]}{dt} = \alpha_1 k_1\left[^{12}CH_3D\right]^2 - k_1\left[^{12}CH_2D_2\right]\left[^{12}CH_4\right] \tag{4}$$

465

466 For simplification, the concentration of $^{12}CH_4$ is set to unity ($[^{12}CH_4] = 1$), making what follows all

467 relative to $^{12}CH_4$. We also invoke the approximation that $\alpha_1 k_1[^{12}CH_3D]^2$ is a constant. This is justified

468 since the concentration of $^{12}CH_2D_2$ relative to CH_4 is about 10^{-8} while that of $^{12}CH_3D$ is 10^{-4}, so

469 $[^{12}CH_3D] \gg [^{12}CH_2D_2]$ even when working at the per mil level. In other words, we treat the change in

470 the $[^{12}CH_2D_2]/[^{12}CH_4]$ ratio as a change in $[^{12}CH_2D_2]$ only in the rate equation. With this approximation,

471 and some rearrangements, one obtains the solution to the differential equation as being

472

$$[^{12}CH_2D_2]_t = [^{12}CH_2D_2]_{EQ} + \left|\left[^{12}CH_2D_2\right]_o - \left[^{12}CH_2D_2\right]_{EQ}\right| e^{-kt} \tag{5}$$

474   .
475
476 where t is the time of the observation, the EQ subscript indicates equilibrium, and the o subscript

477 indicates the initial value. Notice that as $t \rightarrow \infty$, Equation (x) reduces to $[^{12}CH_2D^2]_t = [^{12}CH_2D_2]_{EQ}$. This

478 equation can be further rearranged into a more convenient form by dividing through by the equilibrium

479 concentration of CH_2D_2, yielding

$$\frac{[^{12}CH_2D_2]_t - [^{12}CH_2D_2]_{EQ}}{\left[^{12}CH_2D_2\right]_o - \left[^{12}CH_2D_2\right]_{EQ}} = e^{-kt} \tag{6}$$

480

481   The left-hand side of Equation (x) is the fractional approach to equilibrium. The analogous exchange

482   reaction for $^{13}CH_3D$ is

483
$$^{12}CH_3D + ^{13}CH_4 \underset{k_2}{\overset{\alpha_2 k_2}{\rightleftarrows}} \ ^{13}CH_3D + ^{12}CH_4 \tag{7}$$
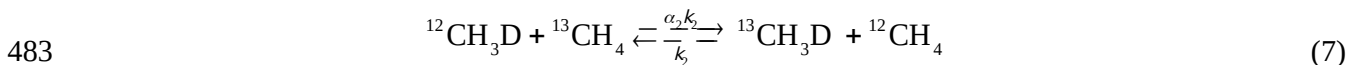
484

485   and results in

486
$$\frac{[^{13}CH_3D]_t - [^{13}CH_3D]_{EQ}}{\left[^{13}CH_3D\right]_o - \left[^{13}CH_3D\right]_{EQ}} = e^{-k_2 t} . \tag{8}$$

487   The form of Equations (7) and (8) show that if the rate constants are the same, and so the e-folding

488   times being $\tau_i = 1/k_i$ are the same, then the relative rates of equilibration depend on the degree of

489   disequilibrium. For example, for an initial gas -50‰ out of equilibrium in $\Delta^{12}CH_2D_2$ and -2‰ out of

490   equilibrium in $^{13}CH_3D$, after $t = 2\tau$, we obtain $\Delta^{12}CH_2D_2 = $ -7‰ relative to equilibrium (a total shift of

491   +43‰) and $^{13}CH_3D$ is -0.3‰ relative to equilibrium (a total shift of +1.6‰). So, if the rate constants

492   for D/H exchange, for example, are the same for the two isotopologues, we should see much larger

493   shifts in $^{12}CH_2D_2$ relative to those in $^{13}CH_3D$, but, when the former is at equilibrium, the latter should be

494   also.

495   We find that unequal rate constants are required to explain our data if the methane prior to re-

496   equilibration was in equilibrium at the lower temperatures suggested by the highest $\Delta^{13}CH_3D$ values.

497   Indeed, for such initial conditions, we calculate that the rate for re-equilibrating $\Delta^{12}CH_2D_2$ would have

498   to be 5 to 10 times that of $\Delta^{13}CH_3D$ to explain a nearly-horizontal relationship as observed in Figure 7.

499   Whether such large difference of re-equilibration rates between the two isotopologues is likely or not

500   will have to be explored in future experimental work. However, based on an analysis of the rates of

501   equilibration based on the symmetry numbers for reactants and transition states (see Labidi et al., 2020

502   and Supplementary material), we conclude that one should not expect k_1/k_2 (i.e., the rate constant for

503    $^{12}CH_2D_2$ relative to that for $^{13}CH_3D$) to be not larger than 2. With this constraint, fitting the SoM data

504 suggests that the initial mass-18 isotopologue composition was below the equilibrium curve (Fig. 7).

505 An initial composition such as this for a microbial gas is not unreasonable given the propensity of

506 microbial methanogenesis to produce low $\Delta^{12}CH_2D_2$ values in general, even in some marine

507 environments (e.g., Ash et al., 2019).

508

509 *6. Implications for the use of methane isotopologues as geothermometers*

510 Three pathways for methane generation (abiotic, thermogenic and microbial) are generally

511 expected to be controlled by kinetic effects rather than by thermodynamic equilibrium. It is thus

512 remarkable that in many instances in nature, especially for thermogenic gases, the 'clumped'

513 composition appears consistent with bond equilibrium. Hence, assessing whether such equilibrium is

514 inherited: 1) from the formation of the methane itself; or 2) from isotopic bond-order re-equilibration

515 under conditions and timescales that remain to be defined, is critical for understanding the true meaning

516 of 'clumped'-based temperatures. In the first case, the 'clumped' composition may accurately record

517 the formation temperature of the methane, whereas in the second case, it is overprinted by a re-

518 equilibration temperature experienced at a point in time in the thermal history of the gas.

519 We suggest that pristine $\Delta^{13}CH_3D$ and $\Delta^{12}CH_2D_2$ signatures inherited from methane generation,

520 in particular of microbial methanogenesis, have been fully or partially overprinted by re-equilibration

521 within the subsurface of the SoM. This conclusion thus supports the idea that in sedimentary reservoirs,

522 isotopologue equilibrium might sometimes be reached after CH_4 formation. The timescales for re-

523 equilibration remain to be established. Though these rates certainly depend on the associated

524 mineralogy as well as on the presence of H-bearing molecules, they likely scale with temperature

525 (Stolper et al., 2017). This suggests that 'clumped'-based temperatures are more prone to record the

526 highest temperatures experienced by the gases. Considering that thermogenic gases are formed

527 continuously during burial, thus spanning a wide range of temperatures, methane formed at lower

22

528 temperatures eventually re-equilibrates to the highest temperature reached. This hypothesis would

529 explain why temperatures derived from 'clumped' isotopologues for thermogenic gases often match the

530 maximum burial temperatures (Stolper et al., 2014, 2017).

531   On the other hand, data from sedimentary reservoirs in Southwest Ontario and Michigan basins

532 (Giunta et al., 2019) show considerable $\Delta^{12}CH_2D_2$ disequilibrium, illustrating a mixing relationship

533 between thermogenic and microbial methane (see Fig. 4). Those disequilibrium signatures are similar

534 to those observed in laboratory cultures, and suggests that re-equilibration in these reservoirs was

535 limited (if any), thus contrasting with the Marmara system studied here. A possible explanation is that

536 samples from Southwest Ontario and Michigan basins come from sedimentary units that never

537 experienced temperatures greater 40-50 °C. We thus speculate that an activation temperature exist,

538 below which rates for re-equilibration are too slow for significant effects on $\Delta^{13}CH_3D$ and $\Delta^{12}CH_2D_2$

539 over geological timescales. Identifying threshold temperatures would help define where to expect re-

540 equilibration of microbial methane that is generally formed at lower temperatures than thermogenic

541 gases. From our data, isotopologue equilibrium measured for samples of apparent microbial origin,

542 samples DV05-PE02, DV04-PE04 and PE08, indicates that re-equilibration to temperatures down to

543 90 °C likely occurs. Not withstanding that re-equilibration rates are likely a function of *in situ* chemical

544 and mineralogical conditions, the contrasting results of these two studies may in turn suggest that a

545 temperature of 40-50 °C is not sufficient for significant re-equilibration of methane isotopic bond

546 ordering.

547

548 **5/ Conclusion**

549   We measured $\Delta^{13}CH_3D$ and $\Delta^{12}CH_2D_2$ from methane-rich cold seeps emanating at the seafloor

550 of the sea of Marmara (SoM). The variability observed among the samples further demonstrates the

551 occurrence of a multitude of distinct gas reservoirs in the subsurface of the SoM, which is consistent

552 with previous observations based on gas geochemistry (Ruffine et al., 2018b), as well as on seismic

553 imaging (Geli et al., 2018).

554 Although $\Delta^{13}CH_3D$ and $\Delta^{12}CH_2D_2$ have been recently used to infer the dominant production

555 mechanism (including sometimes, formation temperature) or mixing relationship between different

556 sources of methane (e.g. Giunta et al., 2019), here we show that methane isotopologues signatures in

557 the SoM cannot be simply explained by mixing. Instead, methane effusing from the SoM seafloor

558 appear to be affected, to varying degrees, by bond re-equilibration, a process in which the isotope

559 bond-ordering inherited from the formation of the methane is subsequently 're-set' to thermodynamic

560 equilibrium during residence at sufficiently high temperatures. This conclusion may suggest that

561 apparent isotopologue equilibrium like overwhelmingly displayed among thermogenic gases (Stolper et

562 al., 2014, 2015, 2017; Wang et al., 2015; Young et al., 2017; Giunta et al., 2019) can in some cases be

563 acquired after formation and therefore, that isotopologue apparent temperatures may trace re-

564 equilibration temperatures rather than the actual formation temperature.

565

572

573

574

575

576 **Appendices**
577 **Isotopologue relationship to temperature**
578 The relationship between $\Delta^{13}CH_3D$ and $\Delta^{12}CH_2D_2$ and temperature can be predicted through *ab initio*
579 calculations (e.g. Ma et al., 2008; Webb and Miller, 2014; Liu and Liu, 2016). In this study, we used the
580 recent expressions proposed by Young et al., (2016, 2017):

582 $\Delta^{13}CH_3D$ (T) $\approx 1000 \ln (1 + 0.0355502/T - 433.038/T^2 + 1270210.0/T^3 - 5.94804$ x $10^8/T^4 + 1.196630$
583 x $10^{11}/T^5 - 9.07230$ x $10^{12}/T^6$)   A.1

585 and

587 $\Delta^{12}CH_2D_2$ (T) $\approx 1000 \ln (1 + 0.183798/T - 785.483/T^2 + 1056280.0/T^3 + 9.37307$ x $10^7/T^4 - 8.919480$ x
588 $10^{10}/T^5 + 9.901730$ x $10^{12}/T^6$)   A.2

590 where T is in Kelvin. The differences between the different computational methods to predict
591 relationship between Δ values and temperatures are less than the analytical uncertainties (Webb and
592 Miller, 2014; Liu and Liu, 2016, Young et al., 2017).

593
594
595
596
597
598
599
600
601
602
603
604
605
606
607
608
609
610
611
612
613
614
615
616
617
618
619

References

Alexander, R., Kagi, R. I., & Larcher, A. V. (1982). Clay catalysis of aromatic hydrogen-exchange reactions. *Geochimica et Cosmochimica Acta*, *46*(2), 219-222.

Ambraseys, N. N., & Jackson, J. A. (2000). Seismicity of the Sea of Marmara (Turkey) since 1500. *Geophysical Journal International*, *141*(3), F1-F6.

Armijo, R., Meyer, B., Barka, A., de Chabalier, J. B., Hubert-Ferrari, A., & Cakir, Z. (2000). The fault breaks of the 1999 earthquakes in Turkey and the tectonic evolution of the Sea of Marmara: a summary. *The 1999 İzmit and Düzce earthquakes: preliminary results*, 55-62.

Ash, J., Egger, M., Treude, T., Kohl, I., Cragg, B., Parkes, R. J., ... & Young, E. D. (2019). Exchange catalysis during anaerobic methanotrophy revealed by 12CH2D2 and 13CH3D in methane. *Geochemical Perspective Letters*, *10*, 26-30.

Bernard, B. B., Brooks, J. M., & Sackett, W. M. (1976). Natural gas seepage in the Gulf of Mexico. *Earth and Planetary Science Letters*, *31*(1), 48-54.

Berner, U., and Faber, E., 1996, Empirical carbon isotope/maturity relationships for gases from algal kerogens and terrigenous organic matter, based on dry, open-system pyrolysis: Organic Geochemistry, v. 24, no. 10-11, p. 947-955.

Bourry, C., Chazallon, B., Charlou, J. L., Donval, J. P., Ruffine, L., Henry, P., ... & Moreau, M. (2009). Free gas and gas hydrates from the Sea of Marmara, Turkey: Chemical and structural characterization. *Chemical Geology*, *264*(1-4), 197-206.

Çağatay, M. N., Yıldız, G., Bayon, G., Ruffine, L., and Henry, P., 2018, Seafloor authigenic carbonate crusts along the submerged part of the North Anatolian Fault in the Sea of Marmara: Mineralogy, geochemistry, textures and genesis: Deep Sea Research Part II: Topical Studies in Oceanography.

Cao, X., Bao, H., & Peng, Y. (2019). A kinetic model for isotopologue signatures of methane generated by biotic and abiotic CO2 methanation. *Geochimica et Cosmochimica Acta*, *249*, 59-75.

Clayton, C. (1991). Carbon isotope fractionation during natural gas generation from kerogen. *Marine and petroleum geology*, *8*(2), 232-240.

Crémière, A., Pierre, C., Blanc-Valleron, M. M., Zitter, T., Çağatay, M. N., & Henry, P. (2012). Methane-derived authigenic carbonates along the North Anatolian fault system in the Sea of Marmara (Turkey). *Deep Sea Research Part I: Oceanographic Research Papers*, *66*, 114-130.

Douglas, P. M. J., Stolper, D. A., Smith, D. A., Anthony, K. W., Paull, C. K., Dallimore, S., ... & Sessions, A. L. (2016). Diverse origins of Arctic and Subarctic methane point source emissions identified with multiply-substituted isotopologues. *Geochimica et Cosmochimica Acta*, *188*, 163-188.

Eldridge, D. L., Korol, R., Lloyd, M. K., Turner, A. C., Webb, M. A., Miller, T. F., & Stolper, D. (2019). Comparison of Experimental vs. Theoretical Abundances of 13CH3D and 12CH2D2 for Isotopically Equilibrated Systems From 1-500° C. *ACS Earth and Space Chemistry*.

Gasperini, L., Polonia, A., Bortoluzzi, G., Henry, P., Le Pichon, X., Tryon, M., Cagatay, N., and Geli, L., 2011, How far did the surface rupture of the 1999 Izmit earthquake reach in Sea of Marmara?: Tectonics, v. 30.

Géli, L., Henry, P., Zitter, T., Dupré, S., Tryon, M., Çağatay, M. N., ... & Natalin, B. (2008). Gas emissions and active tectonics within the submerged section of the North Anatolian Fault zone in the Sea of Marmara. *Earth and Planetary Science Letters*, *274*(1-2), 34-39.

670

671 Géli, L., Henry, P., Grall, C., Tary, J. B., Lomax, A., Batsi, E., ... & Sengör, A. M. C. (2018). Gas and seismicity within the
672 Istanbul seismic gap. *Scientific reports*, *8*(1), 6819.

673

674 Giunta, T., Young, E. D., Warr, O., Kohl, I., Ash, J. L., Martini, A., ... & LaRowe, D. E. (2019). Methane sources and sinks
675 in continental sedimentary systems: New insights from paired clumped isotopologues 13CH3D and 12CH2D2. *Geochimica*
676 *et Cosmochimica Acta*, *245*, 327-351.

677

678 Gonzalez, Y., Nelson, D.D., Shorter, J.H., McManus, J.B., Dyroff, C., Formolo, M., Wang, D.T., Western, C.M. and Ono, S.,
679 2019. Precise measurements of 12CH2D2 by tunable infrared laser direct absorption spectroscopy. Analytical Chemistry,
680 91(23), pp.14967-14974.

681

682 Gruen, D. S., Wang, D. T., Könneke, M., Topçuoğlu, B. D., Stewart, L. C., Goldhammer, T., ... & Ono, S. (2018).
683 Experimental investigation on the controls of clumped isotopologue and hydrogen isotope ratios in microbial methane.
684 *Geochimica et Cosmochimica Acta*, *237*, 339-356.

685

686 Gürgey, K., Philp, R., Clayton, C., Emiro lu, H., and Siyako, M., 2005, Geochemical and isotopic approach to
687 maturity/source/mixing estimations for natural gas and associated condensates in the Thrace Basin, NW Turkey: Applied
688 Geochemistry, v. 20, no. 11, p. 2017-2037.

689

690 Gürgey, K. (2009). Geochemical overview and undiscovered gas resources generated from Hamitabat petroleum system in
691 the Thrace Basin, Turkey. *Marine and Petroleum Geology*, *26*(7), 1240-1254.

692

693 Head, I. M., Jones, D. M., & Larter, S. R. (2003). Biological activity in the deep subsurface and the origin of heavy oil.
694 *Nature*, *426*(6964), 344.

695

696 Holler, T., Widdel, F., Knittel, K., Amann, R., Kellermann, M. Y., Hinrichs, K. U., ... & Wegener, G. (2011). Thermophilic
697 anaerobic oxidation of methane by marine microbial consortia. *The ISME journal*, *5*(12), 1946-1956.

698

699 Inagaki, F., Hinrichs, K. U., Kubo, Y., Bowles, M. W., Heuer, V. B., Hong, W. L., ... & Kaneko, M. (2015). Exploring deep
700 microbial life in coal-bearing sediment down to~ 2.5 km below the ocean floor. *Science*, *349*(6246), 420-424.

701

702 James, A.T. and Burns, B.J., 1984. Microbial alteration of subsurface natural gas accumulations. AAPG Bulletin, 68(8),
703 pp.957-960.

704

705 Kashefi, K., & Lovley, D. R. (2003). Extending the upper temperature limit for life. *Science*, *301*(5635), 934-934.

706

707 Labidi, J., Young, E. D., Giunta, T., Kohl, I. E., Seewald, J., Tang, H., ... & Früh-Green, G. L. (2020). Methane thermometry
708 in deep-sea hydrothermal systems: evidence for re-ordering of doubly-substituted isotopologues during fluid cooling.
709 *Geochimica et Cosmochimica Acta*.

710

711 Luff, R., & Wallmann, K. (2003). Fluid flow, methane fluxes, carbonate precipitation and biogeochemical turnover in gas
712 hydrate-bearing sediments at Hydrate Ridge, Cascadia Margin: numerical modeling and mass balances. *Geochimica et*
713 *Cosmochimica Acta*, *67*(18), 3403-3421.

714

715 Martini, A. M., Walter, L. M., Budai, J. M., Ku, T. C., Kaiser, C. J., & Schoell, M. (1998). Genetic and temporal relations
716 between formation waters and biogenic methane: Upper Devonian Antrim Shale, Michigan Basin, USA. *Geochimica et*
717 *Cosmochimica Acta*, *62*(10), 1699-1720.

718

Prinzhofer, A., & Pernaton, E. (1997). Isotopically light methane in natural gas: bacterial imprint or diffusive fractionation?. *Chemical Geology*, *142*(3-4), 193-200.

Reeves, E. P., Seewald, J. S., & Sylva, S. P. (2012). Hydrogen isotope exchange between n-alkanes and water under hydrothermal conditions. *Geochimica et Cosmochimica Acta*, *77*, 582-599.

Ruffine, L., Dennielou, B., Giovanni, B., Namik, Ç. M., Grall, C., Jean-Luc, C., ... & Etoubleau, J. (2012). *Geochemical dynamics of the natural-gas hydrate system in the Sea of Marmara, offshore Turkey*. INTECH Open Access Publisher.

Ruffine, L., Ondreas, H., Blanc-Valleron, M. M., Teichert, B. M., Scalabrin, C., Rinnert, E., ... & Donval, J. P. (2018a). Multidisciplinary investigation on cold seeps with vigorous gas emissions in the Sea of Marmara (MarsiteCruise): Strategy for site detection and sampling and first scientific outcome. *Deep Sea Research Part II: Topical Studies in Oceanography*, *153*, 36-47.

Ruffine, L., Donval, J. P., Croguennec, C., Burnard, P., Lu, H., Germain, Y., ... & Madre, D. (2018b). Multiple gas reservoirs are responsible for the gas emissions along the Marmara fault network. *Deep Sea Research Part II: Topical Studies in Oceanography*, *153*, 48-60.

Ruffine, L., Germain, Y., Polonia, A., de Prunelé, A., Croguennec, C., Donval, J. P., ... & Grall, C. (2015). Pore water geochemistry at two seismogenic areas in the Sea of Marmara. *Geochemistry, Geophysics, Geosystems*, *16*(7), 2038-2057.

Sattler, A. (2018). Hydrogen/Deuterium (H/D) exchange catalysis in alkanes. *ACS Catalysis*, *8*(3), 2296-2312.

Sessions A. L., Sylva S. P., Summons R. E. and Hayes J. M. (2004). Isotopic exchange of carbon-bound hydrogen over geologic timescales. Geochim. Cosmochim. Acta 68, 1545–1559

Schoell, M. (1988). Multiple origins of methane in the Earth. *Chemical geology*, *71*(1-3), 1-10.

Shuai, Y., Douglas, P. M., Zhang, S., Stolper, D. A., Ellis, G. S., Lawson, M., ... & Hu, G. (2018). Equilibrium and non-equilibrium controls on the abundances of clumped isotopologues of methane during thermogenic formation in laboratory experiments: Implications for the chemistry of pyrolysis and the origins of natural gases. *Geochimica et Cosmochimica Acta, 223*, 159-174.

Stolper, D. A., Sessions, A. L., Ferreira, A. A., Neto, E. S., Schimmelmann, A., Shusta, S. S., ... & Eiler, J. M. (2014). Combined 13 C–D and D–D clumping in methane: Methods and preliminary results. *Geochimica et Cosmochimica Acta, 126*, 169-191.

Stolper, D. A., Lawson, M., Davis, C. L., Ferreira, A. A., Neto, E. S., Ellis, G. S., ... & Sessions, A. L. (2014). Formation temperatures of thermogenic and biogenic methane. *Science*, *344*(6191), 1500-1503.

Stolper, D. A., Martini, A. M., Clog, M., Douglas, P. M., Shusta, S. S., Valentine, D. L., ... & Eiler, J. M. (2015). Distinguishing and understanding thermogenic and biogenic sources of methane using multiply substituted isotopologues. *Geochimica et Cosmochimica Acta*, *161*, 219-247.

Stolper, D. A., Lawson, M., Formolo, M. J., Davis, C. L., Douglas, P. M., & Eiler, J. M. (2017). The utility of methane clumped isotopes to constrain the origins of methane in natural gas accumulations. *Geological Society, London, Special Publications, 468*, SP468-3.

767 Taenzer, L., Labidi, J., Masterson, A. L., Feng, X., Rumble III, D., Young, E. D., & Leavitt, W. D. (2020). Low Δ12CH2D2
768 values in microbialgenic methane result from combinatorial isotope effects. *Geochimica et Cosmochimica Acta*, *285*, 225-
769 236.
770
771 Takai, K., Nakamura, K., Toki, T., Tsunogai, U., Miyazaki, M., Miyazaki, J., ... & Horikoshi, K. (2008). Cell proliferation at
772 122 C and isotopically heavy CH4 production by a hyperthermophilic methanogen under high-pressure cultivation.
773 *Proceedings of the National Academy of Sciences*, *105*(31), 10949-10954.
774
775 Tang, Y., Perry, J. K., Jenden, P. D., & Schoell, M. (2000). Mathematical modeling of stable carbon isotope ratios in natural
776 gases. *Geochimica et Cosmochimica Acta*, *64*(15), 2673-2687.
777
778 Teichert, B. M. A., Chevalier, N., Gussone, N., Bayon, G., Ponzevera, E., Ruffine, L., & Strauss, H. (2018). Sulfate-
779 dependent anaerobic oxidation of methane at a highly dynamic bubbling site in the Eastern Sea of Marmara (Çinarcik
780 Basin). *Deep Sea Research Part II: Topical Studies in Oceanography*, *153*, 79-91.
781
782 Tissot, B., & Welte, D. H. (1978). Petroleum occurrence and formation.
783
784 Treude, T., Boetius, A., Knittel, K., Wallmann, K., & Jørgensen, B. B. (2003). Anaerobic oxidation of methane above gas
785 hydrates at Hydrate Ridge, NE Pacific Ocean. *Marine Ecology Progress Series*, *264*, 1-14.
786
787 Wang, Z., Schauble, E. A., & Eiler, J. M. (2004). Equilibrium thermodynamics of multiply substituted isotopologues of
788 molecular gases. *Geochimica et Cosmochimica Acta*, *68*(23), 4779-4797.
789
790 Wang, D. T., Gruen, D. S., Sherwood Lollar, B., Hinrichs, K. U., Stewart, L. C., Holden, J. F., ... & Delwiche, K. B. (2015).
791 Nonequilibrium clumped isotope signals in microbial methane. *Science*, *348*(6233), 428-431.
792
793 Wang, D. T., Reeves, E. P., McDermott, J. M., Seewald, J. S., & Ono, S. (2018). Clumped isotopologue constraints on the
794 origin of methane at seafloor hot springs. *Geochimica et Cosmochimica Acta*, *223*, 141-158.
795
796 Whiticar, M. J. (1999). Carbon and hydrogen isotope systematics of bacterial formation and oxidation of methane.
797 *Chemical Geology*, *161*(1-3), 291-314.
798
799 Xia, X., & Gao, Y. (2019). Kinetic clumped isotope fractionation during the thermal generation and hydrogen exchange of
800 methane. *Geochimica et Cosmochimica Acta*, *248*, 252-273.
801
802 Yoshinaga, M. Y., Holler, T., Goldhammer, T., Wegener, G., Pohlman, J. W., Brunner, B., ... & Elvert, M. (2014). Carbon
803 isotope equilibration during sulphate-limited anaerobic oxidation of methane. *Nature Geoscience*, *7*(3), 190-194.
804
805 Young, E. D., Rumble III, D., Freedman, P., & Mills, M. (2016). A large-radius high-mass-resolution multiple-collector
806 isotope ratio mass spectrometer for analysis of rare isotopologues of O2, N2, CH4 and other gases. *International Journal of
807 Mass Spectrometry*, *401*, 1-10.
808
809 Young, E. D., Kohl, I. E., Lollar, B. S., Etiope, G., Rumble Iii, D., Li, S., ... & Sutclife, C. (2017). The relative abundances
810 of resolved l2CH2D2 and 13CH3D and mechanisms controlling isotopic bond ordering in abiotic and biotic methane gases.
811 *Geochimica et Cosmochimica Acta*, *203*, 235-264.
812
813
814
815
816

Location	Sample	Ruffine et al., (2018b)			Measured on the Panorama (this study)							
		$\delta^{13}C$ (VPDB)	δD (VSMOW)	C_1/C_{2+}	$\delta^{13}C$ (VPDB)	δD (VSMOW)	$\Delta^{13}CH_3D$	T°C	±	$\Delta^{12}CH_2D_2$	T°C	±
DV1-Central High	DV1-PE02	-43.5	-210	206	-43.3	-207.4	4.59	68.0	4/5	12.00	91.5	9/9
	DV1-PE03	-53	-223	120								
DV2-Western High	DV2-PE01	-44.6	-222	19	-44.6	-220.9	5.00	51.5	4/4	8.47	142	13/15
	DV2-PE02	-44	-229	9	-43.8	-226.1	4.63	66.5	5/5	8.58	140	13/15
DV3-Western flanck Tekirdag	DV3-PE01	-52.3	-214	31	-52.0	-212.3	6.06	16.0	3/3	7.08	169.3	16/19
	DV3-PE02	-57.3	-218	34	n.m	n.m	n.m	n.m		n.m	n.m	
	DV3-PE03	-41.9	-173	10	-41.2	-169.7	3.40	130.5	6/7	9.16	130.3	12/14
	DV3-PE04	-54.8	-216	880	-54.6	-214.0	4.41	76.0	5/5	8.21	146.6	14/15
	DV3-PE06	-52.2	-213	31	-51.9	-210.7	3.99	96.5	6/6	5.77	201.5	21/25
	DV3-PE09	-58.4	-215	1560	-58.0	-214.2	6.30	9.0	3/3	11.25	100.5	10/11
DV4-Southeastern flanck Tekirdag	DV4-PE02	-63.8	-210	5285	-63.8	-208.1	4.29	81.5	5/6	11.61	96	10/10
	DV4-PE07	-66.1	-237	19505	-65.8	-235.6	5.13	46.5	4/4	12.27	88.2	9/10
	DV4-PE08	-66	-243	23147	-65.8	-240.8	4.34	79.5	5/5	12.27	88.2	9/10
DV5-Cinarcik Basin	DV5-PE01	-63.5	-253	1853	-63.3	-252.2	3.89	102.0	6/6	7.29	164.8	16/18
	DV5-PE02	-63.1	-251	1456	-62.9	-248.5	3.50	124.5	7/7	8.61	139.5	14/15
	DV5-PE03	-63.8	-248	12314	-63.7	-249.2	5.70	27.0	3/3	8.89	134.8	13/14
	DV5-PE04	-62.1	-228	1437	n.m	n.m	n.m	n.m		n.m	n.m	

851

852

853

854

855

856

857

858

859

860

861

862

863

864

865
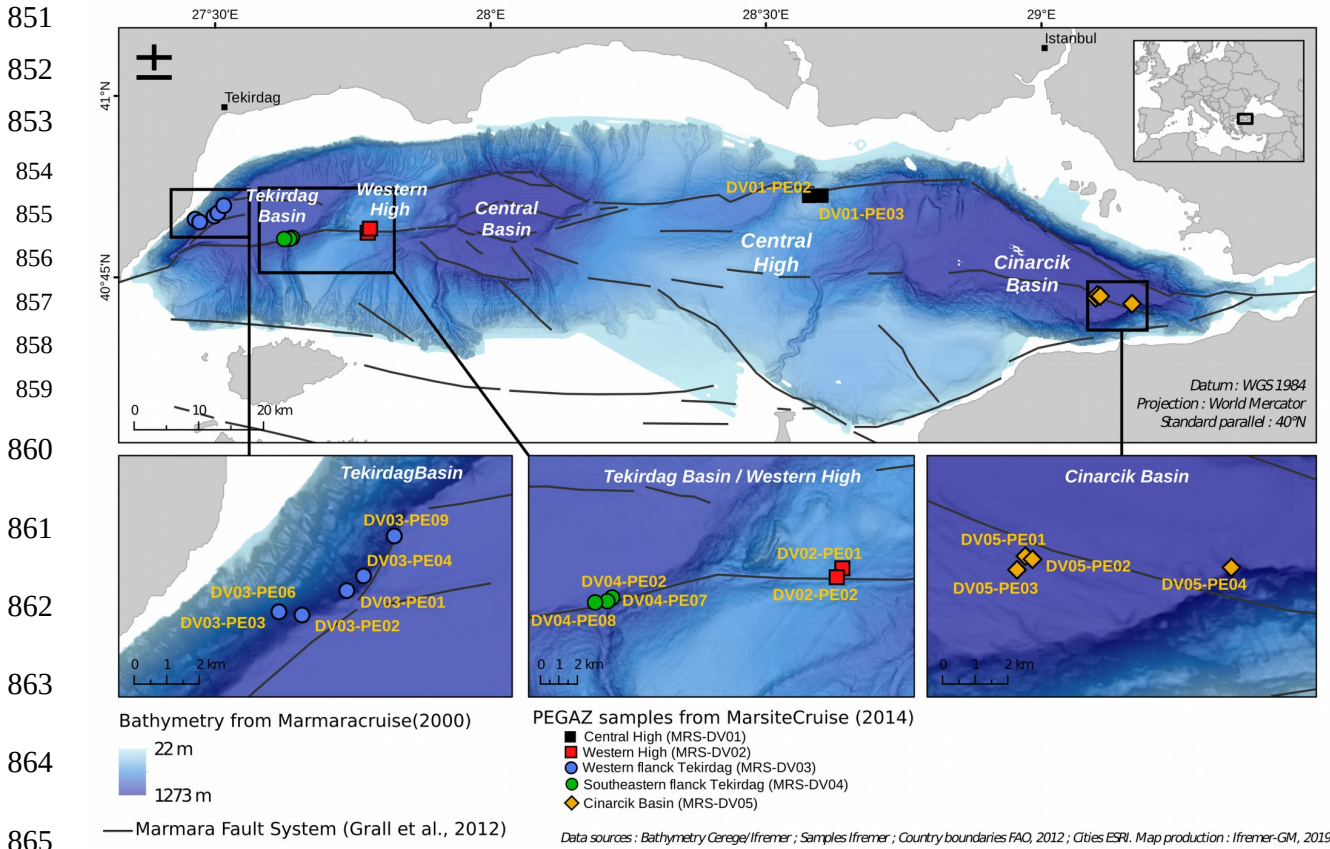
866 ***Figure 1:*** *Map of the sea of Marmara showing the location of the five ROV dives (DV) and gas*
867 *sampling locations.*

868

869

870

871

872

873

874

875

876

877

878

879

880
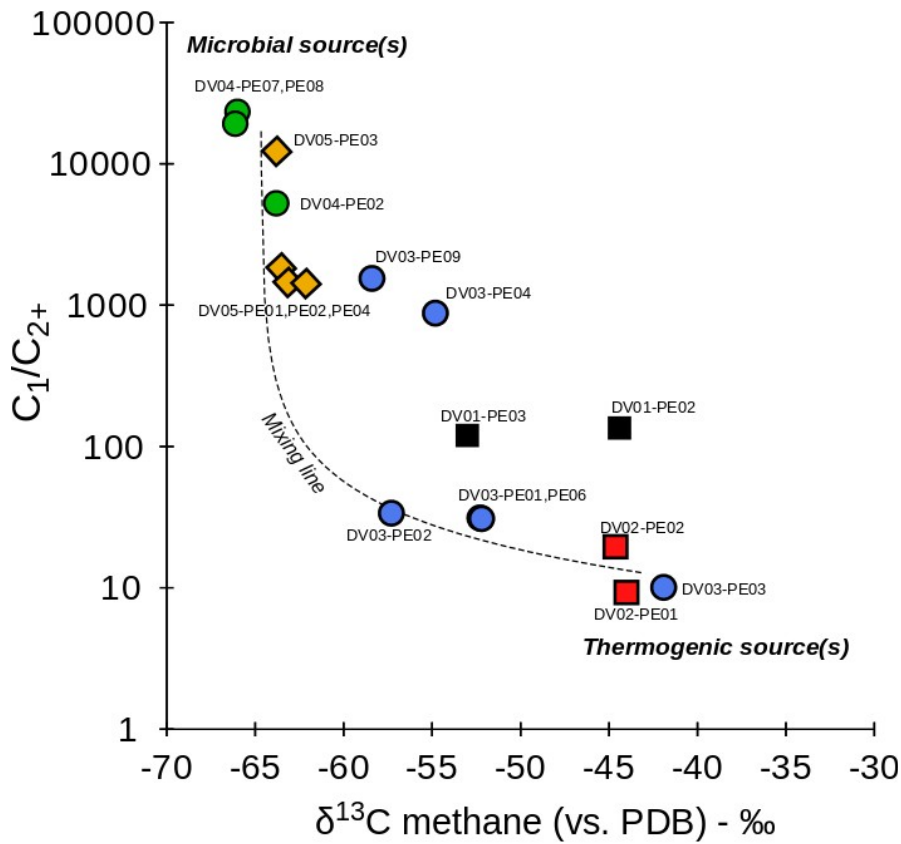
Figure 2: *'Bernard plot' (Bernard et al., 1976): the wetness gas ratio $C_1/(C_2+C_3+C_4)$, is reported as a function of the methane $\delta^{13}C$, together with a hypothetical two-endmembers mixing curve. Data reported here are the same as used in Ruffine et al., (2018b).*
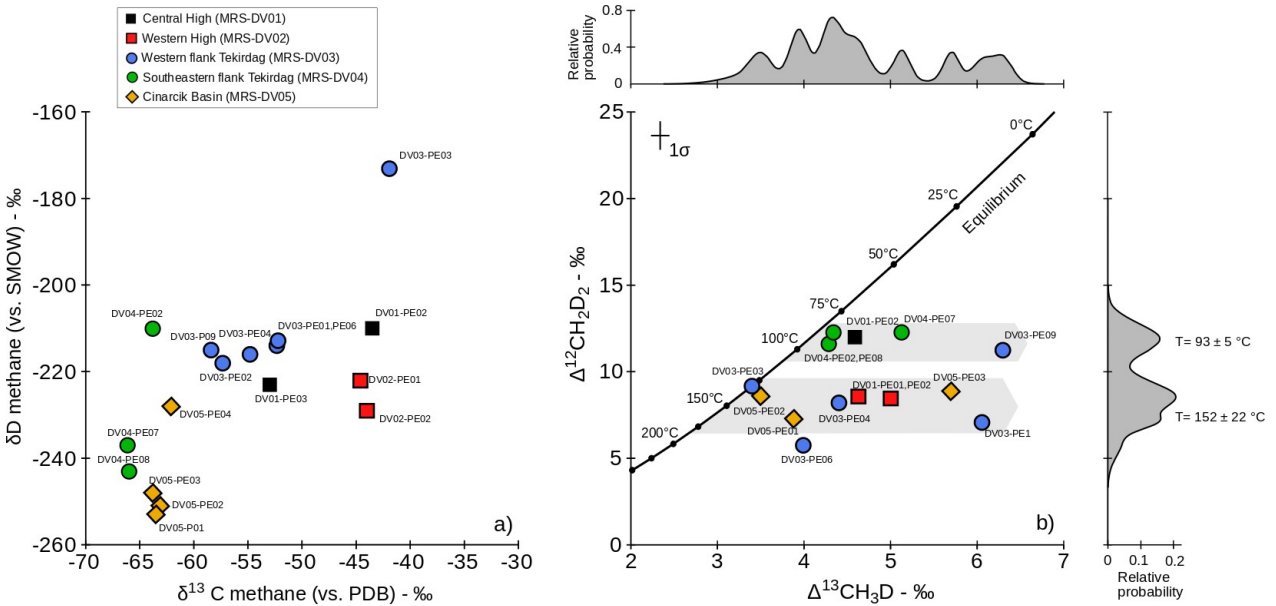
Figure 3: *a) Methane bulk isotope composition. $\delta^{13}C$ and δD measured on the Panorama are within uncertainty of these measurements. b) Methane isotopologue composition for SoM gas samples. The relationship between $\Delta^{13}CH_3D$ and $\Delta^{12}CH_2D_2$ and temperature is calculated following Young et al., (2016, 2017), see details in the Appendix. Despite the disagreement between the temperatures calculated for most samples, the distribution of $\Delta^{12}CH_2D_2$-based temperatures appear to be bi-modal, averaging at 93 ±5 °C and 152 ±22 °C, with few samples matching these temperatures for $\Delta^{13}CH_3D$ as well. Note these two apparent temperatures roughly match the maximum temperatures reached by two of the main source rocks (i.e. organic-rich sediments) in the area, the Eocene Hamitabad Formation and the Oligocene Mezardere Formation (Huvaz et al., 2005; Gürgey, 2009).*
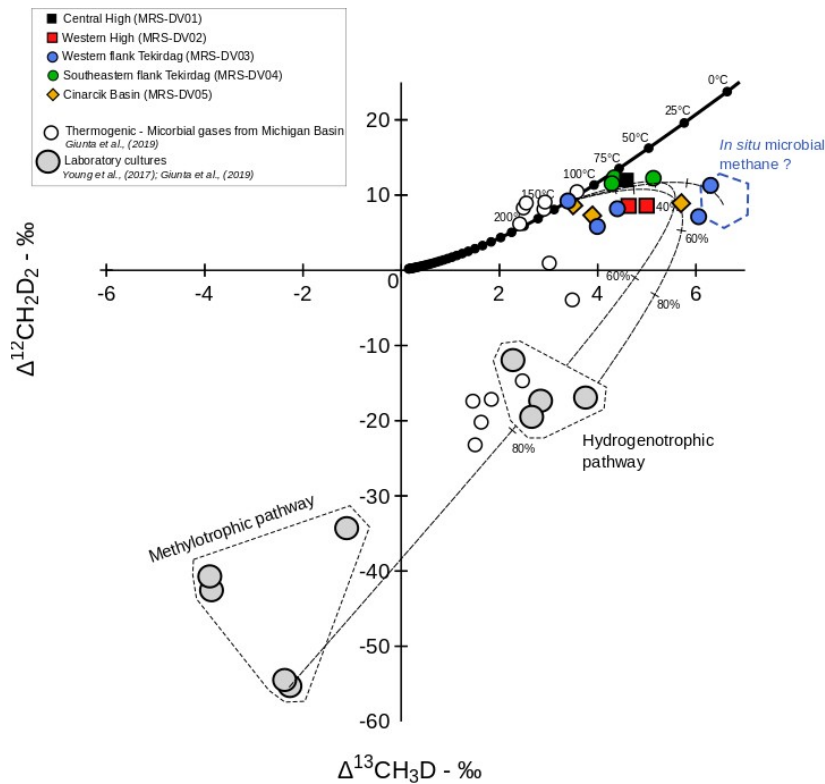
Figure 4: *Methane isotopologue signatures produced by various strains of methanogens using different metabolic pathways (see details in Young et al., 2017; Giunta et al., 2019), shown with gases from the Sea of Marmara (this study) and with thermogenic-microbial gase mixtures from the Michigan Basin (Giunta et al., 2019). Culture of methanogens in laboratory have certainly not explored the whole variability of $\Delta^{13}CH_3D$ and $\Delta^{12}CH_2D_2$ values that can be obtained during microbial generation. Potential mixing curves are given as illustrations, assuming microbial end-members at the SoM are similar to those measured in laboratory. Note that mixing may result in non-linearity effects in the $\Delta^{13}CH_3D$-$\Delta^{12}CH_2D_2$ space (Young et al., 2016; Douglas et al., 2016), with a curvature depending on bulk isotopic compositions ($\delta^{13}C$ and δD) of end-members. With this simple exercise, it is shown that if attempting to fit SoM data with a mixing line having a microbial end-member similar to those measured in laboratory, then SoM gases would at most contain 60% microbial methane which seems inconsistent with extreme C_1/C_{2+} enrichment (>1000). Instead, the data would suggest an in situ microbial end-member with a $\Delta^{13}CH_3D$ of at least 6 ‰, in line with other observations of microbial methane in the deep biosphere (Wang et al., 2015; Inagaki et al., 2015; Ash et al., 2019).*
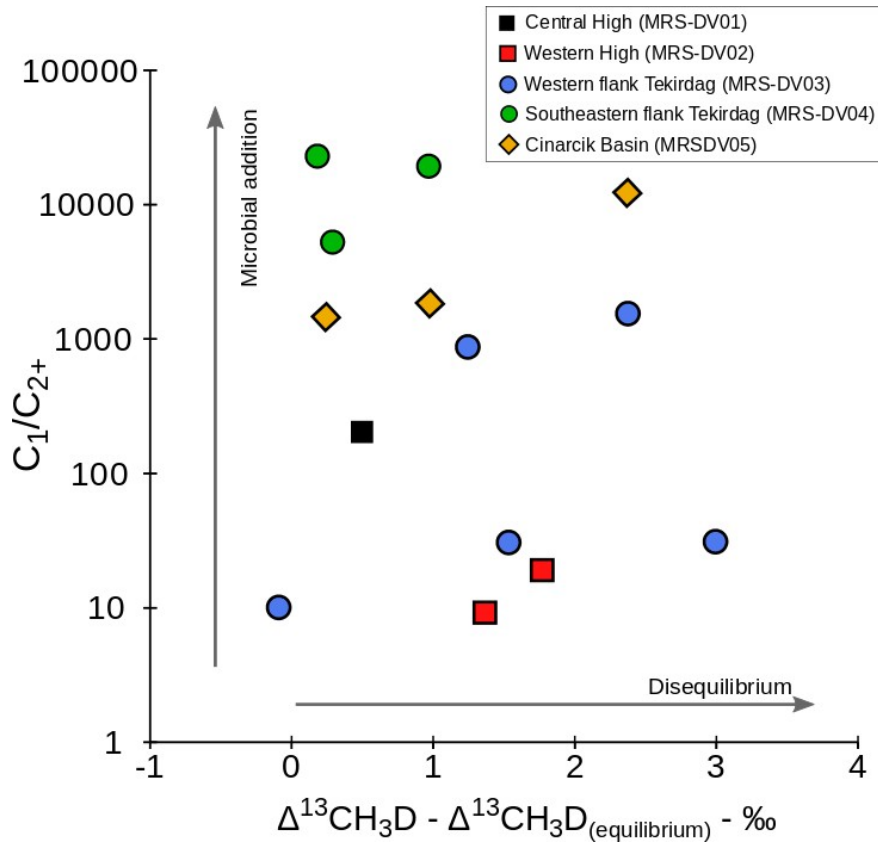
Figure 5: *Wetness ratio (C1/C2+) reported as a function of $\Delta^{13}CH_3D$ - $\Delta^{13}CH_3D_{(equilibrium)}$.*
$\Delta^{13}CH_3D_{(equilibrium)}$ is calculated such as it matches the equivalent temperature inferred from $\Delta^{12}CH_2D_2$.
This is a convenient way to evaluate for each sample, the offset from the equilibrium in the $\Delta^{13}CH_3D$-
axis, and to demonstrate that there are no apparent correlation with C_1/C_{2+}. Assuming that microbial
methanogenesis should produce disequilibrium, as shown in all laboratory culture experiments (Wang
et al., 2015; Stolper et al., 2015; Douglas et al., 2016; Young et al., 2017; Gruen et al., 2018; Giunta
et al., 2019), then in case of mixing with a microbial source, one would expect positive relationship
between the two parameters.
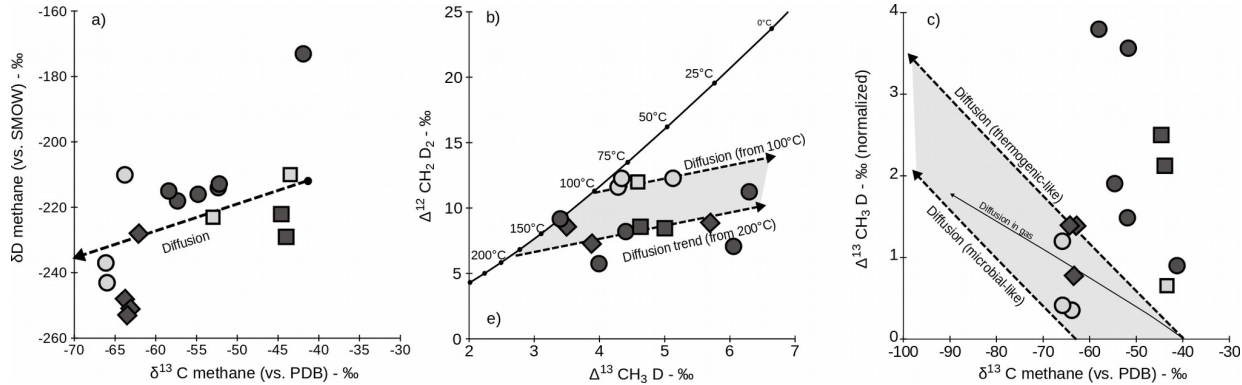
Figure 6: *Investigating the potential role of diffusion on SoM gases. Diffusion trends are plotted by solving the Fick's law in a semi-infinite space for each isotopologue. a) In a bulk $\delta^{13}C$-δD space, diffusion should produce a 1:1 slope. b) In the $\Delta^{13}CH_3D$ - $\Delta^{13}CH_3D$ space, diffusion is also expected to produce a 1:1 slope. The SoM data may suggest two distinct diffusion slopes starting at two different equilibrium temperatures of 100 °C (gray symbols) and 200 °C (dark symbols). c) $\Delta^{13}CH_3D$ as a function of bulk $\delta^{13}C$. Note that $\Delta^{13}CH_3D$ data were normalized to their hypothetical starting equilibrium value, whether at 100 °C (grey symbols) or at 200 °C (dark symbols). The comparison of diffusive effects on singly and doubly-substituted methane isotopologues requires self consistency of diffusion coefficients assigned to each isotopologues. For singly-substituted methane isotopologues, we used $\alpha_{17-16} = D(^{13}CH_4)/D(^{12}CH_4) = D(^{12}CH_3D)/D(^{12}CH_4) = 0.997$, as determined by Prinzhofer and Pernaton, (1997) for diffusion of methane in water. Following the framework of Richter et al., (2006), isotope fractionation factor associated to diffusion may be described as $\alpha_{17-16} = (17/16)^{-\beta}$, where β an empirical parameter depending on the solvent in which diffusion takes place, would thus equals to 0.05. Using this same β value for doubly-substituted isotopologues yields $\alpha_{18-16} = D(^{13}CH_3D)/D(^{12}CH_4) = D(^{12}CH_2D_2)/D(^{12}CH_4) = (18/16)^{-0.05} = 0.994$. Though not considered likely in the context of the SoM, diffusion occurring in gas phase ($\beta = 0.5$) would produce a different diffusion slope in the $\Delta^{13}CH_3D$-$\delta^{13}C$ space. In all cases, the variations observed in $\Delta^{13}CH_3D$ should be associated with much larger variations in bulk $\delta^{13}C$ than they actually are, precluding from considering diffusion as being a major process at play.*
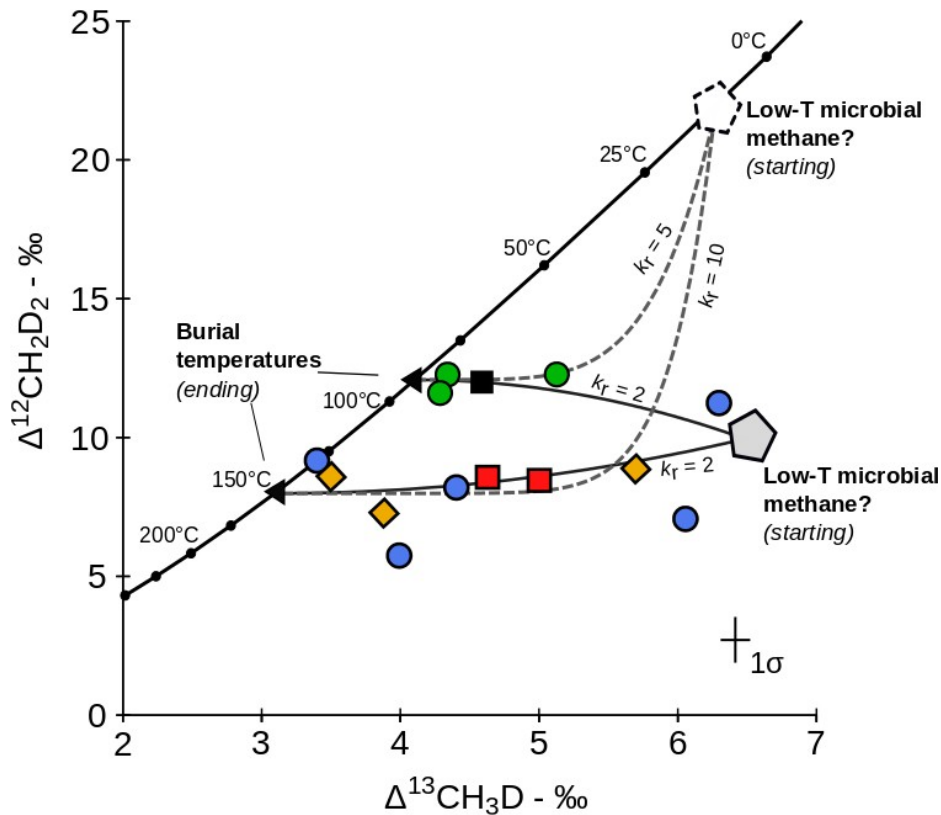
Figure 7: *Exploring the role of different relative rate of re-equilibration. Here we assume that spread to the right of the equilibrium curve reflect partial re-equilibration of $\Delta^{12}CH_2D_2$ and $\Delta^{13}CH_3D$ to burial temperatures of 90 °C and 150 °C. The relative rate is expressed as $k_r = k_{12CH2D2}/k_{13CH3D}$ (or $= k_1/k_2$ in Equations 7 and 8). If assuming a starting isotopologue composition plotting on the equilibrium curve at an equivalent temperature of ~ 10 °C (dashed-pentagon symbol), then k_r is required to be at least of 5 to 10 to explain the data (gray dashed arrows). Alternatively, attempting to fit the data with $k_r = 2$, as suggested by ab initio calculations (see Appendices), implies that methane isotopologue signature prior to re-equilibration was plotting out of the equilibrium curve, perhaps with a $\Delta^{12}CH_2D_2$ signature (coincidentally) not too different from equilibrium 'ending' signatures. For illustration, one possible out-of-equilibrium starting composition is reported here (grey-pentagon symbol) that would allow fitting the SoM data with $k_r = 2$.*